Spectral Features in the AXAF HETGS Effective Area using High Signal Continuum Tests

Herman L. Marshall Daniel Dewey Norbert S. Schulz
Kathryn A. Flanagan

Center for Space Research, M.I.T., Cambridge, MA 02139

ABSTRACT

In order to probe for small scale spectral features of the High Energy Transmission Grating Spectrometer (HETGS) and the Low Energy Transmission Grating (LETG), we performed tests at the AXAF X-Ray Calibration Facility (XRCF) using a very bright continuum source. The Electron Impact Point Source (EIPS) was used with the Cu anode and operated at high voltage and low current in order to provide a bright continuum at high energies. The AXAF CCD Imaging Spectrometer Spectroscopy detector (ACIS-S) was used to discriminate orders and to provide high throughput when operated in continuous clocking (CC) mode. Many spectral features are observed but most of them are emission lines attributable to the source spectrum. We find that the current models for the HETG efficiency, the LETG efficiency and the AXAF High Resolution Mirror Assembly (HRMA) effective area predict very well the observed fine structure near the Au and Ir M edges where the models are most complex. Edges in the detector filter and quantum efficiency (QE) curves are somewhat more sharply defined in the data than in the current models.

By comparing the positive and negative dispersion regions, we find no significant efficiency asymmetry attributable to the gratings and we can further infer that the QEs of the ACIS-S frontside illuminated (FI) chips are consistent to ±10%. On the other hand, we derive the ratio of the QE for the backside illuminated (BI) chips relative to that of the FI chips and show that it deviates from the expected ratio. This deviation may result from grade differences due to operation in CC mode while most calibration data are obtained in timed event mode.

Keywords: AXAF, grating, calibration, X-ray, diffraction

1. INTRODUCTION

Early reports on the efficiencies of the facets used in the High Energy Transmission Grating (HETG) which will be part of NASA's Advanced X-ray Astrophysics Facility (AXAF) are summarized by Dewey et al..[1] These include tests at a synchrotron facility that were used to examine details of the efficiency of small regions on a few reference gratings[2] in order to refine the efficiency model where each grating facet consists of uniform grating bars whose cross section is a simple polygon which is approximately trapezoidal. The HETG Spectrometer (HETGS) includes the AXAF High Resolution Mirror Assembly (HRMA) and the focal plane detector, which is usually the AXAF CCD Imaging Spectrometer Spectroscopy array (ACIS-S). The model of the effective area of the HETGS consists of applying the predicted efficiency of each grating to the effective area of the HRMA at for that grating, combining with the predicted quantum efficiency (QE) of the ACIS-S and then summing over all gratings.[1] A similar approach was used to generate the effective area of the Low Energy Transmission Grating Spectrometer (LETGS), which consists of the HRMA, LETG and the High Resolution Camera Spectroscopy array (HRC-S). Effective area curves, efficiencies, filter transmissions, etc. are available from the AXAF Science Center either in the AXAF Proposer's Guide[3] or on-line at `http://asc.harvard.edu`.

In this paper, we describe tests performed at the AXAF X-ray Calibration Facility[4] which were designed to verify the model of the HETGS effective area. Most of the tests obtained at the XRCF were designed to illuminate the HRMA with a monochromatic beam in order to sample one energy at a time. Reported elsewhere in these proceedings are the results from HETG efficiency model verification using tests with the EIPS using non-flight detectors,[5] tests using the HRC-S as a detector in order to test the predictions of high order efficiencies[6] and tests using the Double Crystal Monochromator[7] in order to examine the HETGS effective area at a wide range of energies. The tests described here employed the Electron Impact Point Source (EIPS) at high voltage and current in order to obtain a

Other author information: Send correspondence to HLM: Email: `hermanm@space.mit.edu`; Telephone: 617-253-8573; Fax: 617-253-8084; WWW: `http://space.mit.edu/ hermanm/`

bright continuum. The continuum was bright enough to obtain 100-1000 counts *per spectrometer resolution element* over most of the useful energy range of the spectrometers. These data could then be used to probe for unexpected spectral features or deviations near the sharp M edges due to the iridium on the HRMA and gold in the gratings. An original purpose of the tests was to test for molecular contamination on the mirrors by examining the mirror Ir M edge decrement, so the tests were given the designation "MC".

The tests proved extremely successful: we found no unusual features in effective area of the HETGS and LETGS to a level of about 5% and found that the models of the Ir and Au M edges agreed to within statistics in all cases. The detailed Ir M edge structure given most recent HRMA effective area curve match the data very well but there is a discontinuity at 2 keV which is not observed. The data were also used to show that the positive and negative orders of the gratings have consistent efficiencies and that the QEs of the frontside illuminated (FI) CCDs in the ACIS-S are all consistent. Finally, using the consistency of the positive and negative orders, we derive the ratio of the QEs of the backside illuminated (BI) CCDs relative to the FI CCDs and show that this ratio does not match the expected ratio of QEs. The reason for this discrepancy may be related to a change of event grades because ACIS was read out in the continuous clocking mode rather than in the timed exposure mode for which most calibration data exist. Finally, a pair of new hot columns (or pixels) was discovered that had not appeared in the preceeding tests.

2. OBSERVATIONS AND DATA REDUCTION

2.1. General

The tests that were reduced are given in table 1, taken at the XRCF on 1997 April 25 between 0341 and 0806 UT. For each of these tests, the EIPS was fitted with the Cu anode set to maximum voltage, 20 kV, and minimum current, 0.1 mA, in order to achieve the highest continuum but keep the total count rate down without using filters. In order to prevent possible radiation induced damage due to the bright zeroth order image, the detector assembly was "dithered" using the five axis manipulator (FAM). A serpentine pattern was used. Long motions in the cross dispersion direction allowed us to reduce the data in large sections at fixed offset along the dispersion direction. Dithering had the advantage of smoothing over detector gaps and any other features.

The ACIS-S was run in the continuous clocking mode and "faint" mode so that three pulse height values were obtained for each event. The detector telemetry limit in this mode is about 393 events/s (see the AXAF Proposer's Guide[3]). As it was, the source was so bright that the ACIS-S telemetry limit was reached easily. Shell quadrants were closed to reduce the count rate to a manageable level during the tests and approximately equal exposure was obtained for all shells.

As described in the AXAF Proposer's Guide,[3] when the telemetry limit is reached, CCD buffers fill and data may be lost. To allow the buffers to empty in each shell quadrant configuration, the mirrors were exposed for 15 min and then closed for 5 min. Exposure is then determined by counting frames, since frames are never only partially lost. The good frames are determined by examining the average counts per frame within the time intervals during which the shutters were open. These time intervals were then examined manually to ensure that closed shutter periods were excluded in the results and to make sure that all good frames were included. The exposure per frame is given by the time to read out 512 rows at 10 μs per column per row and 285 rows per column, giving 1.459 s. The exposure was determined for each CCD separately because the buffers are independent. The pixel boundaries of each chip were transformed into wavelengths by the same method used for the events (see section 2.2) and then both sides were added to obtain the exposure functions shown in figure 1.

Test ID	Grating	HRMA Shells open	Open Quadrant pattern
H-HAS-MC-3.001	HETG	1,3 (HEG subset)	NS, TB
H-HAS-MC-3.005	HETG	4,6 (MEG subset)	T, N, B, S
H-LAS-MC-3.009	LETG	all	T, N, B, S

Table 1. This table shows the set of tests used in the data analysis. For an overview of AXAF calibration, see Weisskopf et al.[4] The HETG high energy gratings (HEGs) have periods near 2000 Å and are arrayed to receive light from the inner pair of HRMA mirrors while the HETG medium energy gratings (MEGs) have periods near 4000 Å and correspond to the outer mirror pair. The quadrant pattern represents the order in which the north (N), south (S), top (T) and bottom (B) quadrants were opened in order to reduce the telemetry saturation.

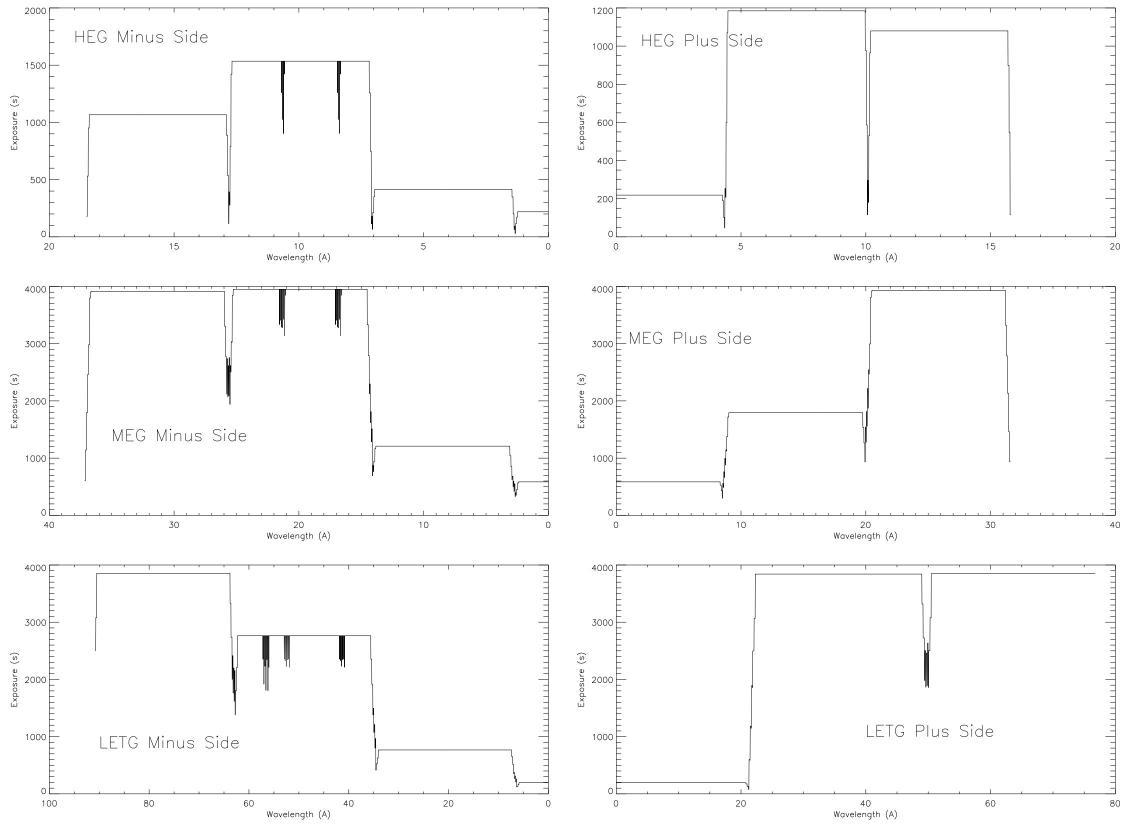

Figure 1. Exposure as a function of wavelength for each test and for the positive and negative orders separated. The details of the tests are given in table 1. Wavelengths are determined from the dispersion relation for an assumed first order spectrum. The ACIS-S CCDs start with S0 on the left and end with S5 on the right. CCD gaps are apparent; the exposure doesn't go to zero due to shifting of the detector assembly along the dispersion direction during the tests. The zeroth order (and origin) was always on the S3 CCD, a backside illuminated (BI) CCD. Several series of shallow dips result from the elimination of columns on the S1 (BI) CCD containing hot pixels and again were shifted to different locations in wavelength space as the detector was moved.

All events from columns containing hot pixels were eliminated from the data and from the exposure function. The hot pixels were most apparent in detector coordinates because the detector was dithered during the observations. Known hot pixels[3] were apparent in the first two observations (3.001 and 3.005) but two new ones showed up in the LETGS observation (3.009) in columns 225 and 232 of the S3 ACIS-S CCD. Another, much milder hot pixel showed up at column 670. The previous hot pixels (columns 383 and 792) were not observed. The new hot columns (or pixels) are somewhat surprising because the test 3.009 immediately followed test 3.005 and the ACIS electonics were not changed.

2.2. Event Processing

The overall event processing approach was the same for each test. First, the details of the dithering were measured and events were shifted to compensate. Both the actual FAM shift in XRCF Y coordinates and the times of the shifts were measured from the centroids of bright emission lines in detector coordinates. The Cu-Kα_1 (8.02783 keV) at $m = +1$ was used for test 3.001, while the $m = +2$ line was used for test 3.005 and the $m = +3$ line of cu-Lα (at 0.9297 keV, or 13.336 Å) was used for test 3.009. These data, shown in figure 2, indicated that the actual FAM Y shifts for all three tests were 0.18 mm, compared to the commanded values of 0.20 mm.* The actual time between Y shifts was observed to be about 561.5 frames, or 819.2 s, which is consistent with the expected value of 820 s.

*Irregularities in the FAM positioning were found in analysis of the HETGS scattering test[8].[9] The sense of the deviation from the commanded motion was 10× smaller and had the opposite sign to the deviation determined here, however.

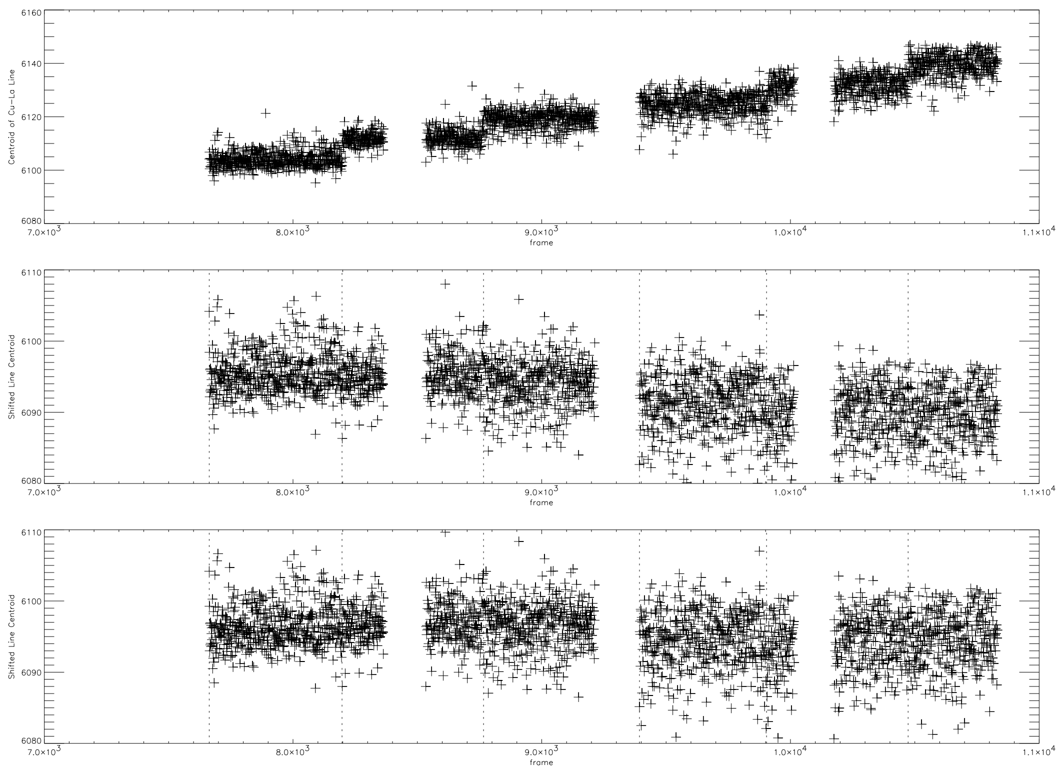

Figure 2. Centroid of the Cu-Lα line (at 13.336 Å) in detector coordinates as a function of ACIS frame (in continuous clocking mode) for test H-HAS-MC-3.005. *Top:* Raw centroids showing the systematic shifts due to dither, where the detector is moved in the $+Y$ direction every 820 s, or 562 frames. *Middle:* Centroids are corrected for shifts of 0.20 mm, which was the commanded value. Dashed lines indicate times when the shifts took place. A residual trend remains, indicating an error in the dither magnitude. *Bottom:* Centroids are shifted by 0.18 mm at each shift time to eliminate the secular drift.

Second, event dispersion distances from zeroth order were computed based on a trial position for the zeroth order (normally determined by the absolute positioning of the FAM). By comparing the positions of lines in the positive and negative sides, the zeroth order position was measured to within a detector pixel (24 μ).

Third, a wavelength, λ_1, for each event was computing under the assumption of first order using the observed dispersion distance for that event and the grating periods, angles and Rowland distances derived from previous XRCF measurements.[5] For the HETGS, the dispersion distances are not directly observed, only the projection along the XRCF Y axis so the projected distance was corrected by $\cos\alpha$, where α is the angle from the dispersion direction to the XRCF Y axis.

Fourth, events are selected by order using the energy, E, computed from the event pulse height. Events were assigned to order m if $|E - hc/(m\lambda_1)| < \delta E$, where h and c are the Planck constant and the speed of light, respectively, and δE is 250 eV (or 150 eV in the case of the LETG observation), larger than the detector energy resolution.

Finally, events were selected according to CCD grade. The CCD grades were determined from the event pulse heights as in timed exposure mode except that only the 3 pulse heights from the event row were available instead of a 3×3 event "island". Thus, certain ACIS grades were not observed, such as those like ASCA grade 2 and 6, which are normally included in the event selection. Similarly, although grades 1 and 5 are normally eliminated in processing, since these grades require detecting corners of the event islands, there were no such grades available. Thus grading had little effect on the event selection.

3. FORMATION AND INTERPRETATION OF THE CONTINUUM SPECTRA

A model of the effective area was generated from a HRMA effective area model recent HETG and LETG efficiency functions, the ACIS-S flight filter model and the ACIS-S FI QE model. All data files used here are available from the AXAF Science Center (ASC) calibration group web page (`http://asc.harvard.edu/cal/cal.html`) and were derived from instrument and telescope team characterizations of the AXAF components.

Because of the high spectral resolution of the grating spectrometers, it is important to use finely gridded models, especially near the spectral features such as the Au M and Ir M edges. The HRMA effective area (EA) was generated by the AXAF telescope science team and is posted to their web site (`http://hea-www.harvard.edu/MST/mirror/www/xrcf/hrma_ea.html`). They adjusted the model of the EA so that the prediction would conform to various XRCF measurements such the SSD continuum data[10] and they incorporated details of Ir reflectivity based on updated optical constants.[11,12] For our purposes, the gradual variation of EA with aperture size will not have a significant effect because we are searching for spectrally small effects, so we used the EA integrated over 2π. The HETGS and LETGS efficiencies incorporate details of the Au edges and are described elsewhere.[1,13] The ACIS flight filter transmission model was fitted to synchrotron data[14] and should include fine structure around the Al and O edges. The ACIS-S CCD QEs are taken from detailed QE curves for two "template" CCDs: one FI chip in the ACIS-I array and one BI chip (S3) in the ACIS-S array[14]; the data from the ASC web page were supplemented with QE values in the 0.05-0.20 keV range with data from a fit to BI QEs by the ACIS/MIT team (see the `QDP` plot of the w134c4r QE on `http://acis.mit.edu`).

Events were binned into histograms before forming a spectrum. The source flux, $f(E)$ (in photon cm^{-2} s^{-1} keV^{-1}), is estimated by combining the data from the positive and negative orders. Denoting the positive side with $+$ and the negative side with $-$, the expected number of counts in a pixel at energy E is given by

$$\begin{aligned} C_+ &= f A \epsilon_+ T Q_+ t_+ dE \\ C_- &= f A \epsilon_- T Q_- t_- dE \end{aligned} \tag{1}$$

where C_- and C_+ are the counts in a pixel at energy E, Q_+ and Q_- are the QEs of the ACIS-S detectors, ϵ_+ and ϵ_- are the efficiencies of the grating into positive and negative orders and are assumed to be equal to ϵ, A is the effective area of the HRMA, T is the transmission of the ACIS-S optical blocking filter, and t_+ and t_- are the exposure times. The quantity dE is the energy width of the pixel based on the derivative of grating dispersion relation (for orders $|m| = 1$) which is very nearly linear:

$$dE = hcE^{-2} P \frac{\delta x}{D} cos(\alpha) \tag{2}$$

where P is the grating period, D is the Rowland distance, and δx is the physical size of an ACIS-S pixel, 0.024 mm. The count spectra for the two sides were combined using an estimator that is not sensitive to situations where the counts on one side were small or zero (due to gaps between CCDs):

$$\hat{f} = \frac{C_+ + C_-}{A \epsilon T dE (Q_+ t_+ + Q_- t_-)} \tag{3}$$

The spectra derived from each test are shown in figures 3, 4, and 5. The Cu-L line series (consisting of α, β, η, ζ, and $\beta_{1,2}$) is quite prominant in all spectra and makes it difficult to search for weak features in the 0.8-1.05 keV region. The Cu-Kα and Kβ lines are apparent at the high energy end so the nearly featureless continuum from 1.05 keV to 7.9 keV could be used for the purposes of this project. The O-Kα and C-Kα lines are also apparent in the MEG and LETG tests and are somewhat broad.

There are features that can be attributed to high orders from the strongest lines, in spite of the pulse height selection. It appears that these high orders can be detected because of a low pulse height tail that extends from the energy of the line down to the background level. These high order lines are especially noticeable in the LETGS spectrum (see figure 5). For example, the Cu-Lα line has an energy of 0.9297 keV but there are a significant number of events with ACIS pulse height energies in the .15 to .45 keV range. When the emission line is dispersed to $m = 4$, the events are dispersed to a distance corresponding to 0.31 keV, where the pulse height selection accepts events in the 0.15-0.45 keV range. The pulse height distribution is discussed again in section 4.

Comparing the spectra obtained from each grating, we see that the continuum and line strengths are very similar but there are systematic deviations. These differences are not the subject of this analysis but may be ascribed to differences between CCD QEs, because each grating places a specific energy onto a different combination of ACIS-S

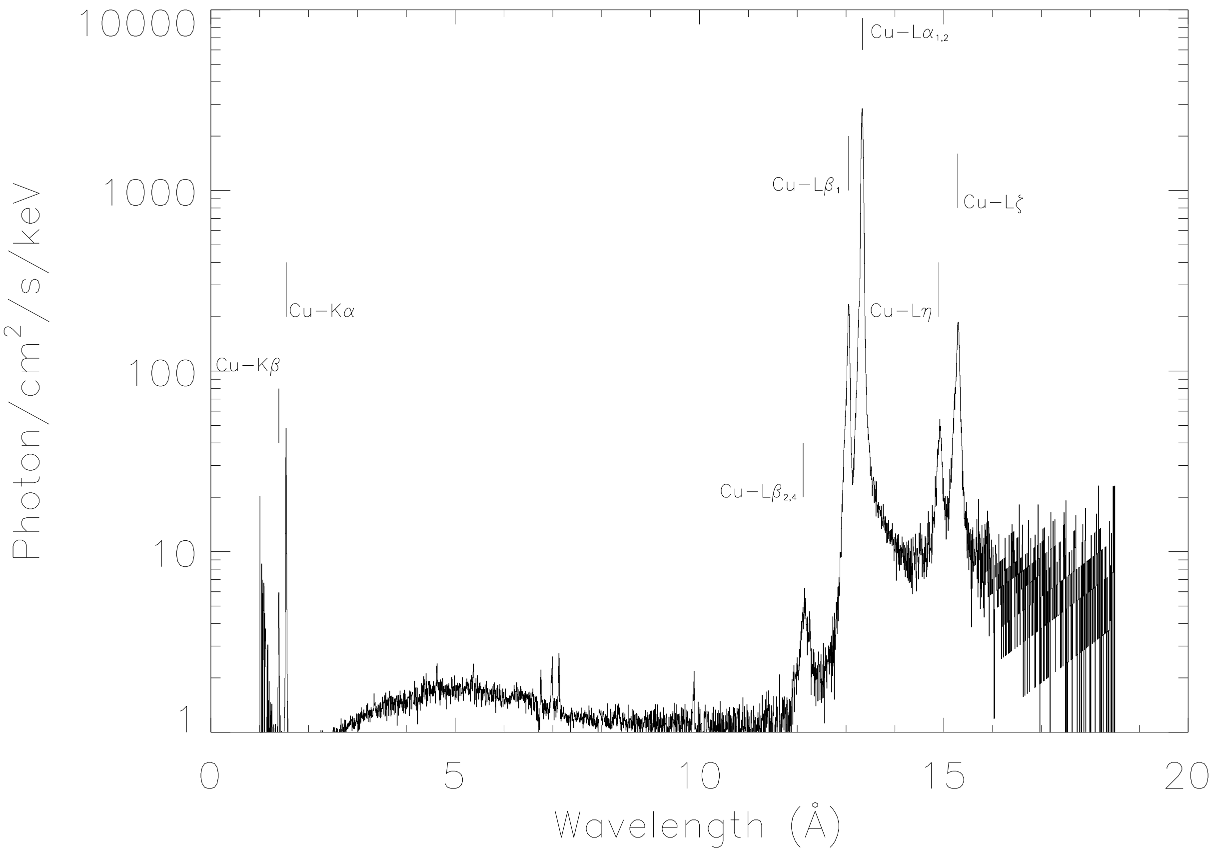

Figure 3. A portion of the spectrum of the source measured by the HEG portion of the HETGS (test H-HAS-MC-3.001). The strong emission lines were easily identified and are marked. The Cu-L lines are broad and have wings that make modelling difficult near them. Weak features are identified in figure 6. The continuum in the range between the Cu-K and Cu-L lines is well fitted with a 10th order polynomial with a few emission lines.

CCDs. In section 4, we show that there are systematic deviations from the expected QE curves using data from within a single grating observation. This issue requires further investigation.

It is clear from the spectra that pileup is not a significant concern when analyzing these data. The peak count rates in the Cu-Lα and Cu-Kα lines gave count rates of order 10 count/s in the HEG observation. For an effective frame time of 0.00285 s in continuous clocking mode, we obtain only 0.03 count/frame, for less than 3% pileup. For the continuum regions, pileup is a factor of >10 less. In the LETGS observation, the Cu-Lα line gives somewhat more counts per frame due to the lower resolution; there is as much as 30 count/s, for at most 10% pileup in this line. Again, the pileup fraction would be less than 1% for most spectral ranges of interest.

We have not yet computed a complete model for the source because the goal of the test was to use the continuum to search for edges and absorption lines which are not part of the source. The continuum shape is not well known *a priori* but is not required for our immediate purpose. The spectrum was estimated empirically from the HEG observations shown in figure 3 by fitting a 10th order polynomial so that we could examine the details of the edge and emission structure in more detail. The data are compared to the model in figure 6. Several emission lines due to contaminants in the source are apparent as deviations from the model. Other deviations are observed at the Al-K and Si-K absorption edges which are in the ACIS-S filter transmission model and the ACIS-S QE model, respectively. The data indicate that the edges are somewhat sharper than predicted. These deviations are caused merely by interpolating the coarsely gridded model files. When more finely computed models are made available,

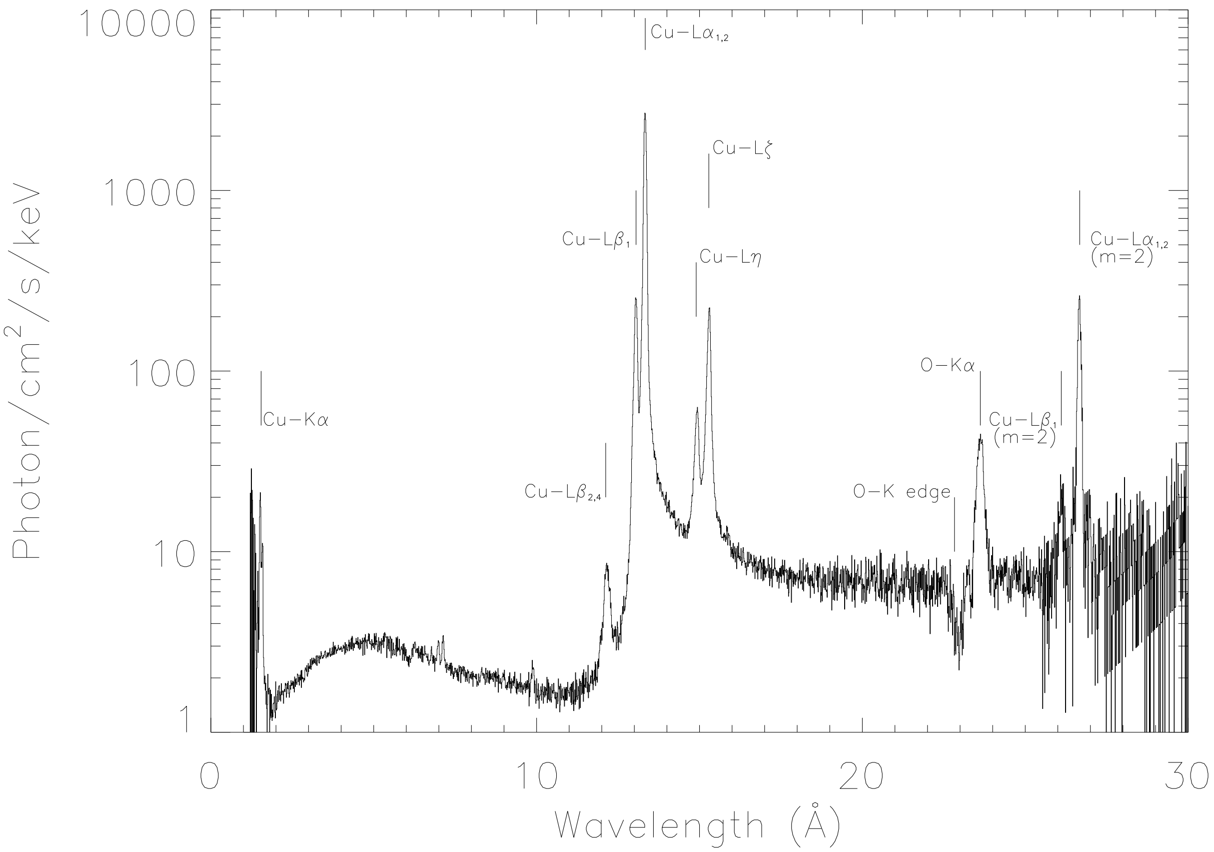

Figure 4. Spectrum of the source measured by the MEG portion of the HETGS (test H-HAS-MC-3.005). The Cu-L α (0.9297 keV), β_1 (0.9498 keV), η (0.832 keV), and ζ (0.8111 keV) are the strongest lines and O-Kα (0.5249 keV) is also easily detected. The line observed at 0.465 keV is actually Cu-Lα observed in second order that is picked up in this first order spectrum due to low pulse height events in the ACIS pulse height distribution. An O-K edge feature is apparent in the 0.53-0.55 keV range.

these edges should be more sharply defined and will be better modeled.

Another feature that is apparent in figure 6 is a deviation at 2 keV. This feature is in the model but not in the data and is caused by a sharp "edge" in the HRMA effective area model. This edge is not physical and was the result of patching newly determined optical constants to older Henke values at this point (R. Edgar, private communication). The feature should be eliminated in the next update to the HRMA effective area.

4. COMPARISON OF POSITIVE AND NEGATIVE SIDES

The ratios of the counts, $R = C_+/C_-$, in the two sides is dependent only on the QEs and the exposure times as long as the grating efficiency is the same for positive and negative orders. All subassembly and XRCF data to date have shown no differences between positive and negative efficiencies, so we may examine the ratios of CCD QEs with these data. We kept track of which CCDs contributed to the ratios so that we could construct $R(E)$. When both orders were on FI CCDs, then all model curves cancel, so that we may test for differences in QEs between FI CCDs or check for grating positive-negative efficiency differences. Figure 7 shows the result. We see that there is remarkable consistency between FI CCDs, especially in the 1.8-2.8 keV region, once we discount the apparent discrepancies due to Cu-L lines. The analysis was designed for regions where the continuum was varying slowly, so

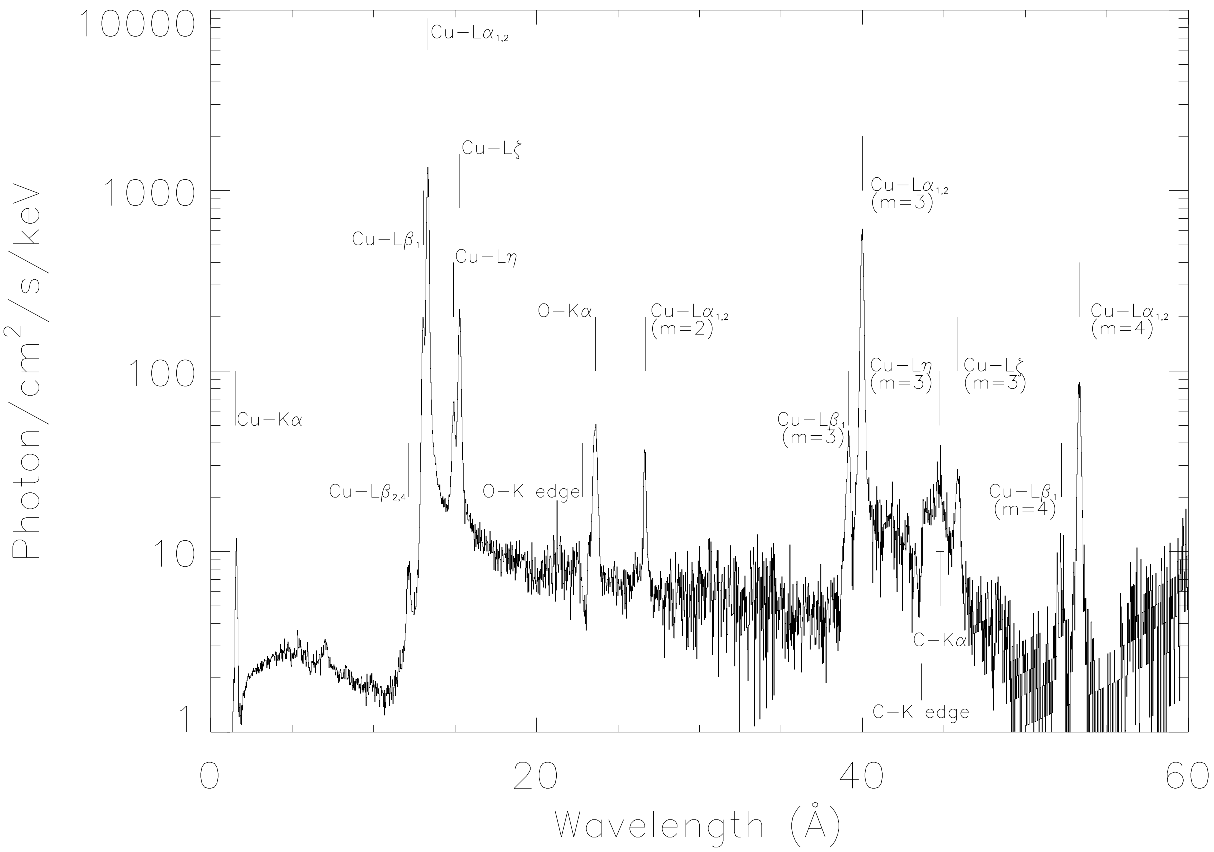

Figure 5. Spectrum of the source measured by the LETGS (test H-LAS-MC-3.009). The Cu-L series is observed in many orders due to the tail of the ACIS pulse height distribution. Note that the $m = 2$ lines are considerably weaker than the $m = 3$ high order lines, as expected for the LETGS. The O-K line is apparent, as in the MEG spectrum, and C-Kα is detected as a broad line component under the $m = 3$ version of Cu-Lη. Note the residual Cu-K edge at 0.28 keV.

it is not too surprizing that the L lines show deviations. These regions should be reduced separately and the effects of pileup should be taken into account.

The ratio of the fluxes determined for the BI CCDs could also be compared to those determined in the FI CCDs. The estimated fluxes already include the ratio of the BI to FI QEs. Figure 8 shows this ratio computed for each grating set. There are very significant, systematic deviations: 15-20% in the 2-4 keV band, 10-40% in the .5-.8 keV band, and differences greater than a factor of 2 below 0.35 keV. The FI QE in the latter region is extremely small and falling rapidly, so it is perhaps not too surprizing that there may be errors there. The fact that the QE ratio may be measured there may be more surprizing.

The deviations elsewhere, and especially in the 2-4 keV range, are more disturbing. Although investigations are in progress, we have identified an effect that may have bearing on this problem. In figure 9, we show the pulse height distribution for events detected by the S3 (BI) CCD and dispersed to a location consistent with energies in the range of 3.0 to 4.0 keV. The figure shows that there is a tail to the pulse height distribution (PHD) that contains a significant number of events and which deviates dramatically from the expected PHD measured from timed exposure mode data. This difference could arise from the inherent limitation of the on-board processing of continuous clocking mode event data. If an event is split such that a significant fraction of the charge appears in an adjacent row, then the event can be detected as two different events when operating in the continuous clocking mode.

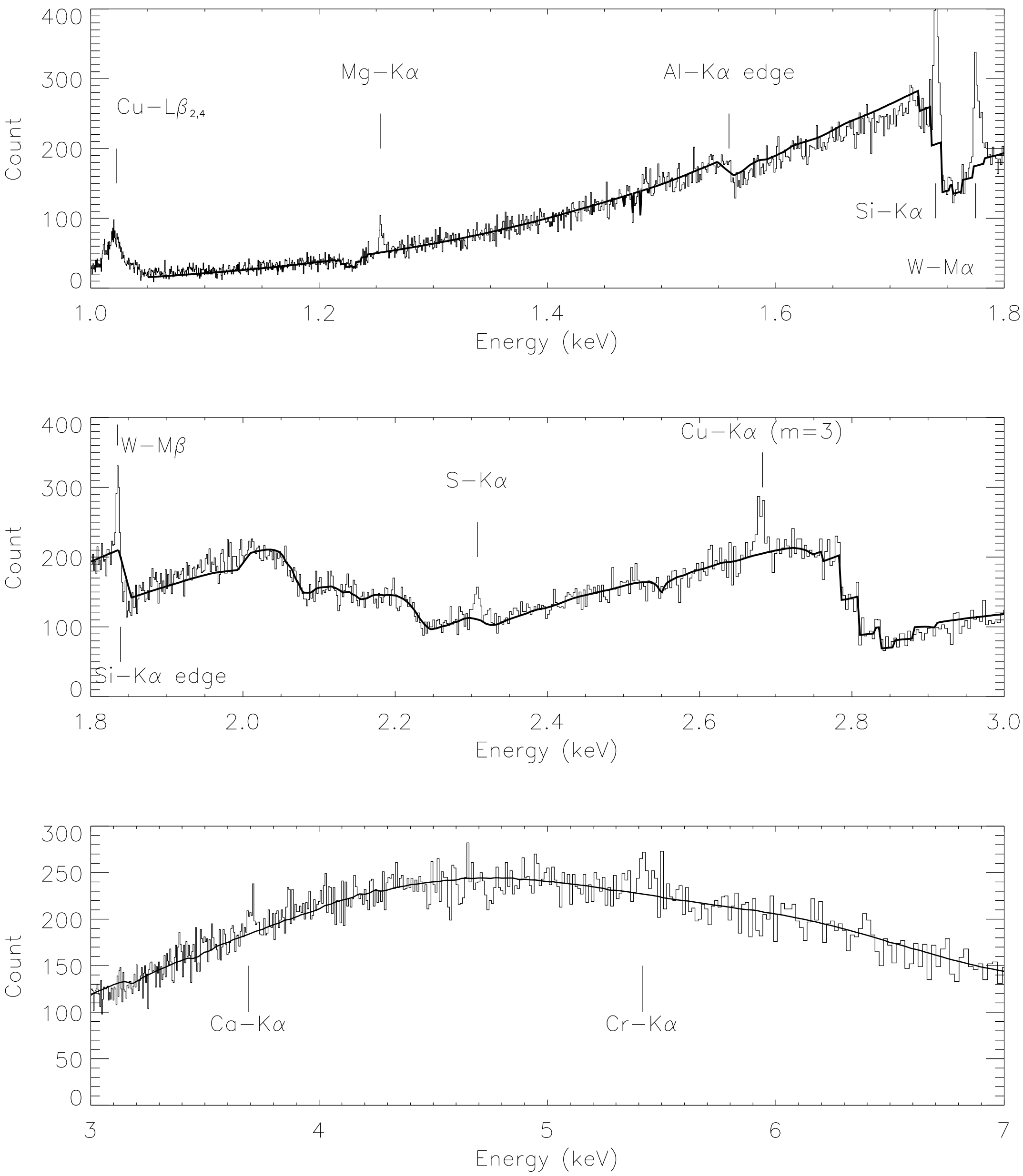

Figure 6. Count spectrum for three separate energy ranges of the test with the HEG portion of the HETGS (test H-HAS-MC-3.001). Emission line features that are intrinsic to the source are marked (e.g. Mg-Kα at 1.254 keV). Two absorption edges are marked (Al-K at 1.559 keV and Si-K at 1.839 keV) where the model of the ACIS-S filter (Al-K) and the detector (Si-K) are so coarsely gridded that the edge does not appear as sharply defined as the data indicate. The bumps and dips from 2.05 through 2.2 keV are the result of Ir M edges in the HRMA effective area and those in the 2.2 to 2.6 keV range arise primarily in the Au M edges of the HEG efficiency curve. Other sharp features are due to exposure variations. A significant deviation from the model occurs at 2.0 keV where the HRMA effective area has a feature that is not tracked by the data.

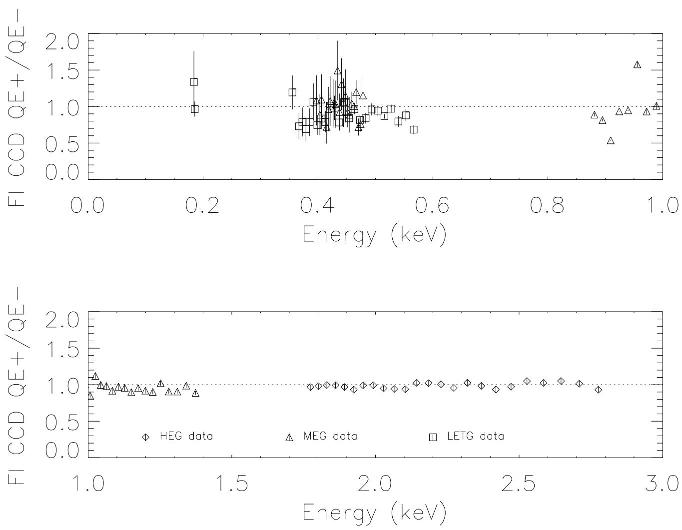

Figure 7. Ratio of the count rates from 30 pixel regions at the same dispersion distance from zeroth order but on two different frontside illuminated (FI) CCDs in the ACIS-S array. The different symbols indicated which grating data set was used to obtain the ratio. The ratios are comfortably close to unity for most of the energy range so that any deviations can be ascribed to variations of QE between FI CCDs. Data from regions near the Cu-L lines should be discounted because the analysis is very sensitive to the exact placement of the integration window around the emission lines. The analysis was designed primarily for regions where the spectrum varies slowly.

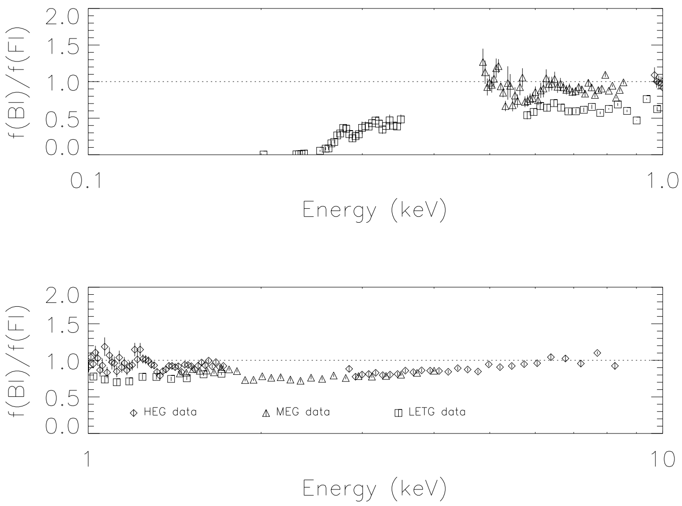

Figure 8. Ratio of the exposure and QE corrected fluxes from 30 pixel regions where the count rate from one side with a BI CCD is compared to that of a FI CCD on the opposite side at the same dispersion distance from zeroth order. The different symbols indicated which grating data set was used to obtain the ratio. This ratio indicates difficiencies in the ratios of the QE models for BI and FI chips. Investigations to explain the observed differences are currently focussed on the differences in event grade assignation between continuous clocking mode and the timed exposure mode normally used in calibration. As in figure 7, data points which are near or include the Cu-L lines should be discounted. Similarly, there is a point at Cu-Kα that is likely to be badly computed.

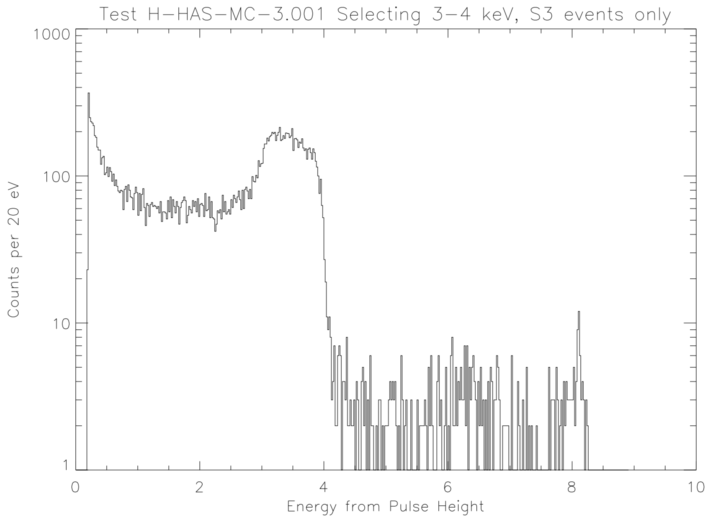

Figure 9. Pulse height distribution (PHD) for a region of the S3 (BI) CCD selected from events whose dispersion corresponds to the 3-4 keV range, assuming $m = 1$ (taken from test H-HAS-MC-3.001). The peak in the 3-4 keV band is expected but the tail that extends to extremely low pulse heights contains much more power than expected. Normally, in timed exposure mode, of order 1% of events would appear in a small peak at 1.74 keV, which is the Si-K escape peak. The escape peak is not visible in this plot because it appears to have been swamped by events with partial charge collection.

5. CONCLUSION AND FURTHER INVESTIGATIONS

These tests provided data that nicely validated the effective area model fine structure near known edges, so that we may be confident that spectral features in the spectrometer can be modelled adequately for observations after AXAF is launched. Concerns arise regarding the HRMA effective area model near 2 keV that will be addressed by the telescope science team. In addition, we noted problems that may result from event loss.

One prospective reanalysis of the data would be to attempt to identify events that are actually associated with split events which were not recognized by the ACIS on-board processor. These events could be combined to improve the pulse height distribution so that the QEs of the BI and FI chips might be more closely comparable to that of timed exposure mode. Very little calibration data were taken in the continuous clocking mode but these data must be examined and modeled to see if the apparent QE differences we find can be explained.

There are grating observations of continuum sources that have yet to be reduced and analyzed. In one test, ACIS was read out in timed exposure mode, so we may be able to compare with the results from these observations. Pileup is expected to be more prevalent, however. Another series of tests involving continuous clocking mode employed the carbon EIPS anode, so data will be available for searching for features in the 0.8-1.1 keV region. A preliminary examination of the data[1] showed slightly different contaminants than observed in these copper anode tests.

These data can still be examined in a bit more detail for possible features in the O-K to Cu-Lζ energy range, spanning from about 0.5 keV to 0.8 keV. The details of the O-K edge structure have been measured at a synchrotron using polyimide filters similar to those used in the MEG, so these details should be incorporated into the HETGS grating efficiency curves.

6. ACKNOWLEDGMENTS

This work was supported in part by NASA under the HETG contract NAS-38249 and the AXAF Science Center contract to the Smithsonian Astrophysical Observatory, NAS8-39073.

REFERENCES

1. Dewey, D., et al, "Towards the Calibration of the HETGS Effective Area," in Grazing Incidence and Multilayer X-ray Optical Systems, Proc. SPIE, vol 3113, pp 144-159, 1997.

2. T.H. Markert et al, "Modeling the Diffraction Efficiencies of the AXAF High Energy Transmission Gratings", in EUV, X-Ray, and Gamma-Ray Instrumentation for Astronomy VI, Proc. SPIE, vol 2518, pp 424-437, 1995.
3. "NASA Advanced X-ray Astrophysics Facility Proposer's Guide," AXAF Science Center technical document ASC.TD.402, 1997.
4. Weisskopf, M.C., et al, "Calibration of the AXAF Observatory: Overview," in Grazing Incidence and Multilayer X-ray Optical Systems, Proc. SPIE, vol 3113, pp 2-17, 1997.
5. Dewey, D., Drake, J.J., Edgar, R.J., Michaud, K., and Ratzlaff, P., "AXAF Grating Efficiency Measurements with Calibrated, Non-imaging Detectors," these proceedings.
6. Flanagan, K.A., Hartner, G.D., Murray, S.S., and Predehl, P., "HETG High Order Diffraction Efficiency," these proceedings.
7. Schulz, N.S., Dewey, D., and Marshall, H.L. "Absolute Effective Areas of the HETGS," these proceedings.
8. Marshall, H.L., et al, "Towards the Calibration of the HETGS Line Response Function," in Grazing Incidence and Multilayer X-ray Optical Systems, Proc. SPIE, vol 3113, pp 160-171, 1997.
9. Davis, J., Marshall, H.L., Dewey, D., and Schattenburg, M. "Analysis and Modeling of the Anomalous Scattering in the AXAF HETGS," these proceedings.
10. Kolodziejczak, J.J., et al., "Uses of continuum radiation in the AXAF calibration, ", in Grazing Incidence and Multilayer X-ray Optical Systems, Proc. SPIE, vol 3113, pp 65-76, 1997.
11. Graessle, D.E., Burek, A.J., Fitch, J.J., Harris, B., Schwartz, D.A., and Blake, R.L., "Optical constants from synchrotron reflectance measurements of AXAF witness mirrors - 2 to 12 keV, " in Grazing Incidence and Multilayer X-ray Optical Systems, Proc. SPIE, vol 3113, pp 52-64, 1997.
12. Graessle, D.E., Blake, R.L., Burek, A.J., Dyson, S.E., Fitch, J.J., Schwartz, D.A., and Soufli, R., "Modeling of synchrotron reflectance calibrations of AXAF iridium-coated witness mirrors over 2-12 keV, " in X-ray Optics, Instruments, and Missions, Proc. SPIE, vol 3444, 1997.
13. Predehl, P., et al, "X-ray Calibration of the Low Energy Transmission Grating Spectrometer: Effective Area," in Grazing Incidence and Multilayer X-ray Optical Systems, Proc. SPIE, vol 3113, pp 172-180, 1997.
14. Bautz, M.W., Nousek, J., Garmire, G., and the ACIS instrument team, "Science Instrument Calibration Report for the AXAF CCD Imaging Spectrometer (ACIS)", available at *http://wwwastro.msfc.nasa.gov/xray/axafps.html*, 1997.